

Radial anisotropy in Valhall from ambient noise surface wave tomography of Scholte and Love wave

Gaurav Tomar^{*1}, Nikolai M. Shapiro¹, Satish Singh¹, Jean-Paul Montagner¹, and Aurelien Mordret²

1. Institut de Physique du Globe de Paris, Sorbonne Paris Cité, CNRS (UMR 7154), Paris, France

2. Earth Resources Laboratory, Department of Earth, Atmospheric and Planetary Sciences, MIT, USA

Summary

We use ambient noise Scholte and Love wave phase velocity tomography to image a few to 100's of meters of the subsurface at the Valhall Oil Field. The noise is recorded by 4D multi-component ocean bottom cables from the Valhall life of field seismic (LoFS) network. We cross-correlate 6.5 hours of continuous recordings between all possible pairs of receivers to extract the Scholte and the Love waves. We use the vertical-vertical (ZZ) component cross-correlations (CC) to extract the Scholte waves and the transverse-transverse (TT) CC to extract the Love waves. We construct 2D Scholte and Love wave phase-velocity maps using the Eikonal tomography method. We then invert these phase velocity maps jointly by using the Neighbourhood algorithm. We invert the local dispersion curve to get 1-D velocity profile at each point in the geographical cell and combine them to obtain a 3-D anisotropic velocity model of Valhall. We get significant negative radial anisotropy ($V_{SH} < V_{SV}$) in shallow layers and positive radial anisotropy ($V_{SH} > V_{SV}$) in the deeper layers.

Introduction

The distribution of anisotropy in the Earth's crust and mantle gives valuable information about its deformation history. Mantle anisotropy is well studied and is believed to principally reflect the lattice preferred orientation of olivine (Montagner and Anderson, 1989; Montager and Tanimoto, 1991). The crustal anisotropy can be caused by a variety of mechanisms including mineral orientation, fine layering within sedimentary or magmatic rocks, or the preferred orientation of faults or cracks (e.g., Shapiro et al., 2004; Jaxybulatov et al., 2014; Mordret et al., 2015). With the development of Ambient Noise Surface-Wave Tomography (ANSWT) (e.g., Shapiro and Campillo, 2004; Shapiro et al 2005; Campillo et al. 2011; Ritzwoller et al. 2011), surface waves can be observed at periods short enough to construct shear wave velocity models at crustal depths and measure their anisotropy.

Shear wave velocities inferred from the Rayleigh waves often differ from those obtained with Love waves. Such incompatibilities are generally considered as a robust diagnostic for the presence of anisotropy in the crust and upper mantle, which is commonly called radial or polarization anisotropy (Muyzert and Snieder, 2000). Radial anisotropy is a property of a medium in which the

speed of the wave depends on its polarization and direction of propagation.

In the exploration seismology the studies to image the subsurface using surface waves have been developing rapidly (Stewart, 2006; Dellinger and Yu, 2009; de Ridder and Dellinger 2011). The study is supported with in-depth analysis (Mordret et al. 2013a,b,c, de Ridder and Biondi, 2013, Mordret et al. 2014a,b) using the ambient noise at Valhall. The Scholte wave phase velocity maps are constructed at Valhall life of the field seismic in Mordret et al. (2013b) by using the Helmholtz tomography (Ritzwoller et al. 2011). A high-resolution isotropic 3D S-wave model in the Valhall oil field up to 600m has been constructed by Mordret et al. (2014a), using the ambient noise surface wave tomography.

The azimuthal anisotropy in the Valhall overburden was estimated in Muyzert et al. (2002) and Mordret et al. (2013c). In this paper after presenting the data and giving a brief introduction of methods, we construct the 2D phase velocity maps of Scholte and Love waves at different periods using the ambient noise cross-correlation between the each pair of receivers and the Eikonal tomography (Lin et al., 2009). We use the local dispersion curve from the Scholte and Love wave phase velocity maps and invert them jointly using Neighbourhood algorithm (NA) to obtain local 1D profile of Valhall and combine all the 1D profile to get 3D radially anisotropic shear wave velocity model of Valhall.

Data and cross-correlations

The Valhall LoFS is a permanent ocean-bottom cables array made of 2320 four-component sensors (a three-component geophone and hydrophone) installed on the seafloor above the Valhall-oil reservoir. The data set used in this study consists 6.5 hours of continuous ambient noise records at vertical (Z), south-north (N) and west-east (E) components of geophones. We have computed more than 10 millions of inter-station cross-correlations and considered NN, EE, NE and EN combinations. We rotated these correlations by using the method discussed in Lin et al. (2008) to get transverse-transverse (TT) and (RR) components. The TT components contain Love waves while the ZZ and the RR components contain Scholte waves. The data set is filtered between 0.5 and 1.85 Hz to construct the phase-velocity maps at different periods. In

Radial anisotropy in Valhall from ambient noise tomography

this range of frequency the noise source is isotropic and the noise records are dominated by the natural secondary microseism (Mordret et al., 2013a).

Ambient noise tomography of Scholte and Love waves

The surface wave tomography is done with using the Eikonal tomography technique (Lin et al., 2009). We construct the 2D phase velocity maps for Scholte and Love wave at different periods. Figure 1 shows the phase velocity maps of Scholte waves at 0.7, 1 and 1.4 s. We compute the frequency-dependent phase travel times from each inter-station noise CC. Then we invert the phase travel time to compute the 2D phase velocity maps for different frequencies, the method for constructing the phase velocity maps is discussed in details in Mordret et al. (2013b). Our results show good consistency with the results obtained in Sirgue et al. (2010) and Mordret et al. (2013b). At 0.7 s (Figure 1a), we find a high velocity anomaly that corresponds to the paleo-channel present. In the south east part of the area a big paleo-channel is clearly visible in the map at 1 s (Figure 1b). A low velocity anomaly is present in the middle of the network in 1 s and 1.4 s maps (square dashed box Figure 1b).

Figure 2 shows the 2D phase velocity maps for Love waves at periods of 0.8, 1 and 1.4 s. The SNR is lower for Love waves than for the Scholte waves. To increase it, we stacked cross-correlations from every four closely located pairs of sensors before applying the Eikonal tomography. The horizontal resolution analysis performed by Mordret et al. (2013b) has shown that the features could be recovered at the scale of 400 m. This indicates that by stacking CC from close pairs of receivers we do not reduce the horizontal resolution in our data set. The depth sensitivity of Love waves is different from the Scholte wave. We can see the large paleo-channel and the low velocity anomaly in the 1.4 s map of 1.4 s (dashed box in Figure 2c). We explore this differential resolution of and invert the 2D phase velocity maps jointly to get the radially anisotropic velocity model of Valhall.

Depth inversion with the Neighbourhood algorithm

We use the Neighbourhood algorithm (NA) developed by Sambridge (1999) to invert the phase velocity maps. The NA is a Monte-Carlo global direct search technique to sample a model-space. The detail of the method that we use here to invert the phase velocity maps are described in Mordret et al. (2014a). The shear wave velocity within top 600 m of the Valhall overburden are modelled using a power law:

$$V_s(d) = V_0((d+1)^\alpha - (d_0+1)^\alpha + 1), \quad (1)$$

where V_s is the shear-wave velocity, d is the depth, V_0 is the velocity at sea floor, α is the power-law parameter and d_0 is the water depth. We construct the phase velocity maps at periods between .7 to 1.6 s with the time interval of .1 s for the Scholte and the Love waves. We parameterize the depth structure in 11 layers. We perform the inversion with the 3 parameters V_0 , α and V_l to get the isotropic model and with the 4 parameters V_0 , α , ψ_1 and ψ_2 (radial anisotropy) to construct a local 1D anisotropic model of Valhall. The radial anisotropy is taken as $2*(V_{SH} - V_{SV}) / (V_{SH} + V_{SV}) * 100\%$. We invert the local fundamental mode phase velocity dispersion curve of Scholte and Love waves jointly to get local 1-D shear wave velocity profiles. First, we perform isotropic inversion jointly using the Scholte and Love wave dispersion curve. Figure 3 shows the result of the isotropic inversion of the local dispersion curve at the position of (x, y = 3.5, 8 Km), we can see that the results of this isotropic inversion do not fit well data in Figure 3a. Therefore, the radial anisotropy is required to explain our data set.

We perform the anisotropic joint inversion of the local dispersion curve taken from the position at (x, y = 3.5, 8 km). Figure 4 shows the results of a joint inversion of Scholte and Love wave dispersion curves. We run the 25000 of models and keep the best-fit 1-D profile for every cell. For each 1-D model we compute a theoretical dispersion curve by using the Herrmann and Ammon (2004) routines and a misfit is calculated between the theoretical and observed to the corresponding cell. The blue line in figure 4 shows the best-fit inverted phase velocity dispersion curve and the red line shows the observed phase velocity dispersion curve from the phase velocity maps for Scholte 4a and Love 4b waves. It can be seen that the inverted dispersion curves fit our data very well with these parameters (Figure 4c). The difference between V_{SV} and V_{SH} defines the radial anisotropy in the medium. We perform the inversion with these parameters for every local dispersion curve in the cell and combined them to get the final 3-D model of the subsurface.

Figure 5 shows the map of the best misfit and the anisotropy parameters maps we get during the inversion for the whole grid. In almost all locations the final misfit is below 0.2 (Figure 5a) indicating that the power-law approximation is a good model for the depth velocity profile. However, in the south-eastern part of the grid, the misfit is high because of the large paleo-channel present at the depth of 200-250 m. The similar behaviour of the power-law model is found in Mordret et al. (2014) for the paleo-channel in the isotropic inversion. The misfit can improved by using the different parameters of inversion for the paleo-channel. We find a negative radial anisotropy up to 18% (Figure 5b) in the layers above 250 m depth where the V_{SV} is greater than the V_{SH} which can be caused by the

Radial anisotropy in Valhall from ambient noise tomography

near vertical cracks and faults similar to the cause of the azimuthal anisotropy observed by Muyzert et al. (2002) and Mordret et al. (2013c). We then observe a prominent positive radial anisotropy (up to 23%) in the deeper layers (Figure 5c) from the depth 250 m to 600 m where V_{SH} is faster than the V_{SV} .

Conclusions

We have constructed a set of 2D phase velocity maps of Scholte and Love waves at different frequencies to image the near surface structure of Valhall with using the Eikonal tomography method. We have inverted these maps to obtain a 3D shear wave velocity model of Valhall area down to depths of ~ 1 km. We could not fit the ensemble of

the data with an inversion based on an isotropic parameterization of the shear velocity model. Therefore, we decided to include the depth-dependent radial anisotropy into our inversion. We found a significant negative radial anisotropy in the shallow layers at Valhall that might be caused by nearly vertical cracks. We also found the positive radial anisotropy in the deeper layers in Valhall.

Acknowledgement

We gratefully acknowledge the support of Schlumberger and Total in this project. We give our sincere thanks BP Nogle AS and Valhall partners Hess Norge AS for granting access the seismic data [and their permission to publish the abstract].

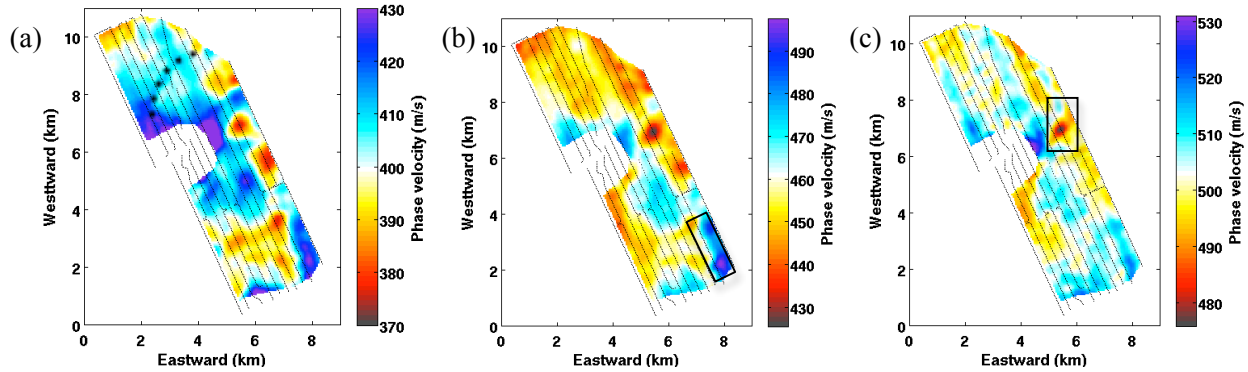


Figure 1: Final phase velocity maps at 0.7 (a), 1.0 (b) and 1.4 s (c) of Scholte wave. The dashed line in (a) indicates the shallow paleo-channel, the rectangle box in (b) indicates the large paleo-channel and the rectangle box in (c) indicate the low velocity anomaly.

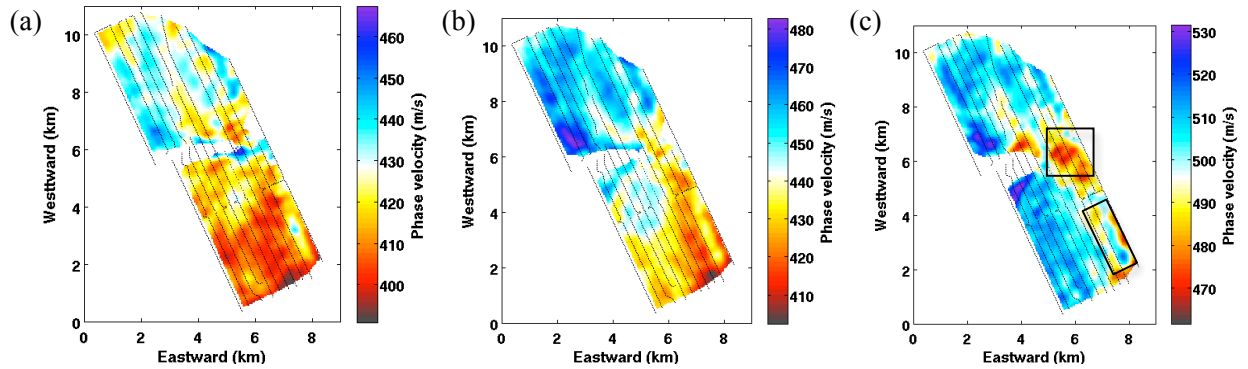


Figure 2: Final phase velocity maps at 0.8 (a), 1.0 (b) and 1.4 s (c) of Love wave. The rectangle box in (c) indicates the large paleo-channel and the square in (c) indicate the low velocity anomaly.

Radial anisotropy in Valhall from ambient noise tomography

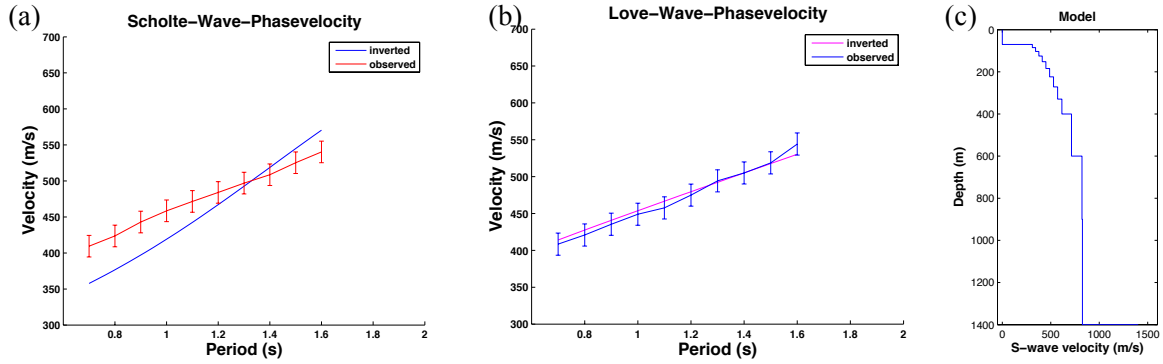


Figure 3: Isotropic joint inversion of local Scholte (a) and Love wave (b) dispersion curve at the position $(x, y) = (3.5, 8)$ Km. (c) isotropic V_s model at that point.

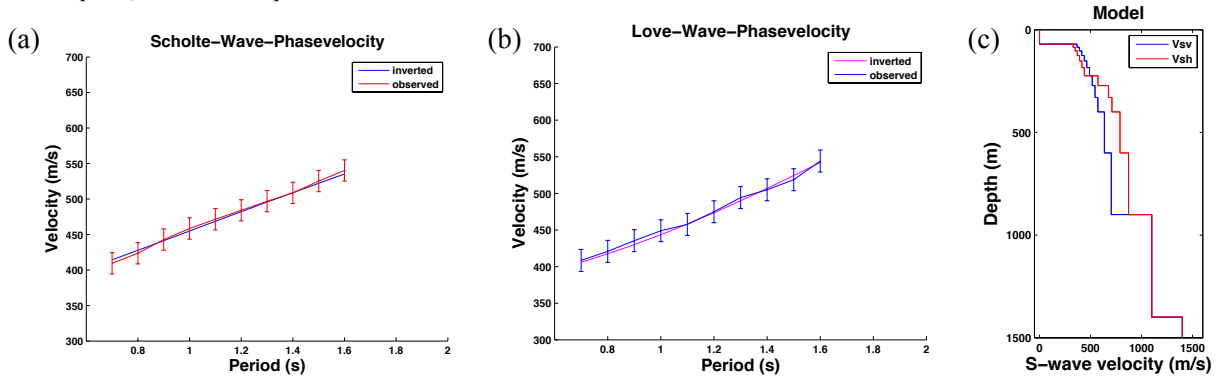


Figure 4: Anisotropic joint inversion of local Scholte (a) and Love wave (b) dispersion curve at the position $(x, y) = (3.5, 8)$ Km. (c) V_{SV} and V_{SH} model in blue and red respectively after inversion.

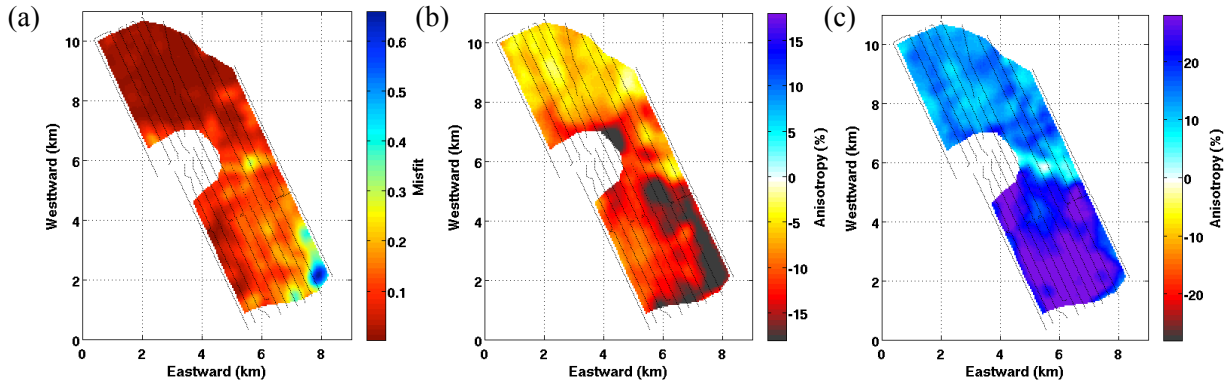


Figure 5: (a) The minimum misfit map after inversion of whole grid of Valhall. (b) The negative anisotropy (%) in the shallow layers up to 250 m and (c) positive anisotropy (%) in the deeper layers from 250 m to 600 m.

Radial anisotropy in Valhall from ambient noise tomography

References

- Campillo, M., Roux, P. and Shapiro, N.M. [2011] Correlation of seismic ambient noise to image and monitor the solid Earth: *Encyclopedia of Solid Earth Geophysics, Springer-Verlag*.
- de Ridder, S., and J. Dellinger [2011], Ambient seismic noise eikonal tomography for near-surface imaging at Valhall, *Leading Edge*, 30(5), 506–512, doi:10.1190/1.3589108.
- de Ridder, S., and B. L. Biondi [2013], Daily reservoir-scale subsurface monitoring using ambient seismic noise; *Geophysical Research Letters*, 40, 1–6, doi:10.1002.
- Dellinger, J. A., and J. Yu (2009), Low-frequency virtual point-source interferometry using conventional sensors, in 71st Meeting, European Association of Geoscientists and Engineers, Expanded Abstracts, p. X047, Amsterdam, Netherlands (conference of the EAGE).
- Herrmann, R. & Ammon, C., 2004. Surface waves, receiver functions and crustal structure, *Computer Programs in Seismology*, 133, 135.
- Jaxybulatov, K., N. Shapiro, I. Koulakov, A. Mordret, M. Landès, and C. Sens-Schönfelder (2014), A large magmatic sill complex beneath the Toba caldera, *Science*, 346(6209), 617–619.
- Lin, F., M.P. Moschetti, and M.H. Ritzwoller [2008] Surface wave tomography of the western United States from ambient seismic noise: Rayleigh and Love wave phase velocity maps, *Geophys. J. Int.*, doi:10.1111/j.1365-246X.2008.03720.x.
- Lin, F.C., Ritzwoller, M.H. & Snieder, R. [2009] Eikonal tomography: surface wave tomography by phase front tracking across a regional broad-band seismic array, *Geophys. J. Int.*, **177**(3), 1091–1110.
- Montagner, J.-P., and D. L. Anderson (1989), Petrological constraints on seismic anisotropy, *Phys. Earth Planet. Inter.*, 54(1–2), 82–105, doi:10.1016/0031-9201(89)90189-1.
- Montagner, J.-P., and T. Tanimoto (1991), Global upper mantle tomography of seismic velocities and anisotropies, *Journal of Geophysical Research: Solid Earth*, 96(B12), 20337–20351, doi:10.1029/91JB01890.
- Mordret, A., Landès, M., Shapiro, N., Singh, S., Roux, P., & Barkved, O., 2013a. Near-surface study at the Valhall oil field from ambient noise surface wave tomography, *Geophysical Journal International*, **193**(3), 1627–1643. 88, 89, 99, 101, 103, 112, 116, 120, 154, 156.
- Mordret, A., Shapiro, N. M., Singh, S. C., Roux, P., & Barkved, O. I., 2013b. Helmholtz tomography of ambient noise surface wave data to estimate Scholte wave phase velocity at Valhall Life of the Field, *Geophysics*, **78**(2), WA99–WA109. 113, 114, 115, 130, 132, 138, 150, 160, 163.
- Mordret, A., Shapiro, N. M., Singh, S., Roux, P., Montagner, J.-P., & Barkved, O., 2013c. Azimuthal anisotropy at Valhall : The Helmholtz equation approach, *Geophysical Research Letters*, **40**, 151, 165.
- Mordret, A., M. Landès, N.M. Shapiro, S.C. Singh, and P. Roux (2014a), Ambient noise surface wave tomography to determine the shallow shear velocity structure at Valhall: depth inversion with a Neighbourhood Algorithm, *Geophys. J. Int.*, 198 (3), 1514–1525, doi: 10.1093/gji/ggu217.
- Mordret, A., N. M. Shapiro, and S. Singh (2014b), Seismic noise-based time-lapse monitoring of the Valhall overburden, *Geophys. Res. Lett.*, 41, 4945–4952, doi:10.1002/2014GL060602.
- Mordret, A., D. Rivet, M. Landès, and N. M. Shapiro (2015), Three-dimensional shear velocity anisotropic model of Piton de la Fournaise Volcano (La Réunion Island) from ambient seismic noise, *J. Geophys. Res. Solid Earth*, 120, doi:10.1002/2014JB011654.
- Muyzert, E., Kommedal, J., Iranpour, K., & Olofsson, B., 2002. Near surface S-velocities, statics, and anisotropy estimated from Scholte waves, in *EAGE 64th Annual Conference & Exhibition*, vol. 28. 58, 88
- Muyzert, E., Snieder, R., (2000), An alternative parameterization for surface waves in a transverse isotropic medium; *Physics of the Earth and Planetary Interiors* 118, 125–133.
- Ritzwoller, M.H., Lin, F.C. & Shen, W. [2011] Ambient noise tomography with a large seismic array, *Comptes Rendus Geoscience*, **343**(8), 558–570.
- Sambridge, M.[1999] Geophysical inversion with a neighbourhood algorithm. Searching a parameter space, *Geophys. J. Int.*, **138**(2), 479–494.
- Shapiro, N. M., and Campillo, [2004] Emergence of broadband Rayleigh waves from correlations of the ambient seismic noise: *Geophysical Research Letters*, **31**, 1615–1619.
- Shapiro, N.M., M.H. Ritzwoller, P. Molnar, and V. Levin [2004] Thinning and Flow of Tibetan Crust Constrained by Seismic Anisotropy, *Science*, 305, 233–236.
- Shapiro, N. M., M. Campillo, M., Stehly, L. and Ritzwoller, M. [2005] High-resolution surface-wave tomography from ambient seismic noise: *Science*, **307**, 1615–1618.
- Sirgue, L., Barkved, O., Dellinger, J., Etgen, J., Albertin, U., & Kommedal, J., 2010. Full waveform inversion : the next leap forward in imaging at Valhall, *First Break*, **28**, 65–70. 29, 31, 32, 33, 76, 78, 99, 101, 134, 141, 142, 147, 150, 152

Radial anisotropy in Valhall from ambient noise tomography

Stewart, P. (2006), Interferometric imaging of ocean bottom noise, SEG Tech. Program Expanded Abstr., 25(1), 1555–1559, doi:10.1190/ 1.2369817.

